

See discussions, stats, and author profiles for this publication at: <https://www.researchgate.net/publication/244479653>

3D Hollow Nanostructures as Building Blocks for Multifunctional Plasmonics

ARTICLE *in* NANO LETTERS · JULY 2013

Impact Factor: 13.59 · DOI: 10.1021/nl401100x · Source: PubMed

CITATIONS

34

READS

50

8 AUTHORS, INCLUDING:



Ermanno Miele

Istituto Italiano di Tecnologia

27 PUBLICATIONS 430 CITATIONS

[SEE PROFILE](#)



M. Patrini

University of Pavia

144 PUBLICATIONS 1,856 CITATIONS

[SEE PROFILE](#)



Enzo Mario Di Fabrizio

King Abdullah University of Science and Techn...

455 PUBLICATIONS 5,792 CITATIONS

[SEE PROFILE](#)



Andrea Toma

Istituto Italiano di Tecnologia

107 PUBLICATIONS 1,170 CITATIONS

[SEE PROFILE](#)

3D Hollow Nanostructures as Building Blocks for Multifunctional Plasmonics

Francesco De Angelis,^{*,†} Mario Malerba,[†] Maddalena Patrini,[‡] Ermanno Miele,[†] Gobind Das,[†] Andrea Toma,[†] Remo Proietti Zaccaria,[†] and Enzo Di Fabrizio^{§,||}

[†]Nanostructures Department, Istituto Italiano di Tecnologia (IIT), 16163 Genova, Italy

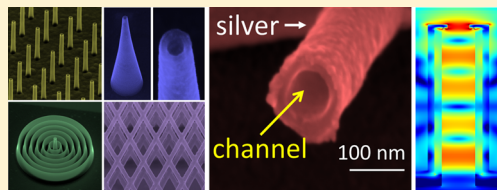
[‡]Dipartimento di Fisica, Università degli Studi di Pavia, Via Bassi 6, 27100 Pavia, Italy

[§]King Abdullah University of Science and Technology (KAUST), Thuwal 23955, Saudi Arabia

^{||}Università degli Studi Magna Graecia di Catanzaro, Viale Europa, 88100 Catanzaro, Italy

S Supporting Information

ABSTRACT: We present an advanced and robust technology to realize 3D hollow plasmonic nanostructures which are tunable in size, shape, and layout. The presented architectures offer new and unconventional properties such as the realization of 3D plasmonic hollow nanocavities with high electric field confinement and enhancement, finely structured extinction profiles, and broad band optical absorption. The 3D nature of the devices can overcome intrinsic difficulties related to conventional architectures in a wide range of multidisciplinary applications.



KEYWORDS: Plasmonics, 3D nanofabrications, nanocavity, nanochannel, Raman, optofluidics

In the past decade, a deep theoretical understanding and a wide range of applications have been proposed in different areas of plasmonics. They include sensing applications through enhanced spectroscopy in the near-infrared and visible range,^{1–6} time-resolved ultrafast spectroscopies^{7,8} plasmonic metamaterials,^{9–13} electrochemical and photochemical catalysis,^{14–17} photovoltaics,¹⁸ nanolaser and spaser,^{19,20} heat delivery,²¹ nano-optical tweezers,^{22,23} AFM and scanning probe spectroscopies,^{24–27} and others. Concurrently, new fields are emerging from distant disciplines such as optofluidics,^{28,29} optoelectronics,^{30,31} and quantum plasmonics.³² Optofluidics is a field in which photonic and microfluidic architectures are integrated to provide enhanced functions and performances with particular attention to chemical and biological analysis.²⁸ Despite optofluidics relies on the delivery of light in small liquid volumes, recent works have highlighted the opportunities offered by this field in sunlight-based fuel production, photobioreactors, and photocatalytic systems.²⁹ On the other hand, optoelectronics aims at developing new systems where optical and electronic properties are synergistically combined to obtain new and powerful functions. In this regards, graphene is one of the most promising candidate materials,³⁰ where several recent results, ranging from solar cells and light-emitting devices to photodetectors and ultrafast lasers, have been shown. However, the implementation of photonic/plasmonic devices in optofluidics and optoelectronics encounters some obstacles which must be overcome for making these fields evolve. In particular, we outline (i) the realization of 3D plasmonic nanocavities able to accumulate the optical energy in a volume where liquid samples can be flowed through and (ii) the realization of plasmonic antennas which can be connected to

electric power sources, without preventing plasmonic functioning (conventional plasmonic antennas are usually electrically isolated). A third severe challenge that hinders the realization of the previous ones, and more in general delays progress in plasmonics and photonics, is the difficulty of realizing large area 3D nanostructures with a well-defined shape and layout. In fact, from one hand top-down approaches are ineffective to produce 3D structures with tunable geometries, whereas bottom-up methods suffer great limitations when 3D nanostructures have to be achieved in whatever 2D layout. These difficulties impose severe limitations on the design of novel and powerful architectures, which are the core of the modern optics.

Here we present a new manufacturing method based on secondary electron lithography generated by ion beam milling. It enables the fabrication of three-dimensional hollow nanostructures with a fine control on the overall geometries and layouts. In the following we describe the fabrication method, giving some examples of the variety of feasible nanostructures, and then we focus our attention on vertical hollow nanopillars.^{33–35} The aim of the latter is to give a more clear idea of the capabilities of the methods and the distinctive features of the proposed 3D nanostructures.

The process is briefly sketched in Figure 1 (further details can be found in Supporting Information section 1). A layer of resist polymer is deposited on a silicon nitride membrane by spin-coating and FIB (focused ion beam) milling is used to define the structure (a cylinder in figure) from the backside of

Received: March 26, 2013

Revised: June 19, 2013

Published: July 1, 2013



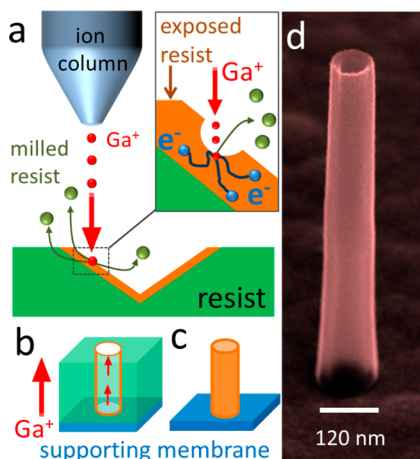


Figure 1. Plasmonic hollow nanostructures fabrication method. (a–c) Sketches representing the fabrications steps. (d) SEM picture of a hollow pillar (resist template): 1.1 μm in height on silicon nitride supporting membrane.

the membrane.^{36–38} During the milling process the interaction between gallium ions and resist polymer produces low-energy secondary electrons (Supporting Information section 2), which are ideal to perform lithographic processes, being effective in breaking carbon–carbon bonding in a region in close proximity to the milled surface (Figure 1a,b). Because of the high secondary electron doses, the lithographic process causes inversion of the resist (from positive to negative tone) in a thin layer of polymer surrounding the milled surface. As a consequence, the overexposed layer becomes insoluble, and when the sample is immersed in a solvent, the unexposed resist is removed whereas the overexposed one remains on the sample (Figure 1c). This layer represents an exact replica of the nanostructure milled by the ion beam, and it can be used as template of the final device. An example is shown in Figure 1d where a nanotube of 1.2 μm in height, external diameter 120 nm, and inner channel diameter 80 nm is shown. The minimum channel size depends on both ion beam current (i.e., beam size) and nanotube height (the higher the nanotube, the larger the channel), but it also strongly depends on the nanostructure shape. For instance, a nanotube of 500 nm in height has a minimum channel size in the order of 50 nm, whereas it can be smaller for a nanoneedle (or nanovolcano, Figure 3 top-center) of few micrometers. As it can be seen, the FIB milling produces a small flare at the template base (increasing of tube radius close to the membrane) that is proportional to the ion beam current. For ion beam parameters used in this work (30 keV, 100 pA) the flare at the base is below 7% of the radius. The typical energy of emitted secondary electrons is in the order of few tens of electronvolts, and their mean free path is tens of nanometers; then the template thickness is typically below 25 nm. When desired, the template thickness can be further thinned by means of oxygen-based RIE (reactive ion etching).

We notice that gallium ion implantation occurs, as consequence of the milling process, in both template layer and supporting membrane.³⁸ Although most of the ions is implanted in a region that is removed by the milling itself, a small fraction of them still contaminates the final device. By using X-ray microanalysis and TEM inspections, we estimated the fraction of gallium contaminating the template to be less than 5% of the total number of atoms (Supporting Information

section 5). This value can be reduced by further optimizing the fabrication process (gas-assisted milling) and annealing postprocessing that promotes gallium desorption. However, despite additional investigations are necessary, we do not expect significant variation of the optical and electronic properties of an amorphous polymer for such a low contamination level.

The FIB exposure is fast, and it can be scaled on large areas. For instance, the exposure of the nanotube shown in Figure 1 takes 300 ms; therefore, more than 10^4 structures can be fabricated in 1 h exposure. The employment of large-area commercial FIB systems (higher ion beam currents, superior performances, and faster beam blanker) together with the process optimization (in particular, the choice of more sensitive resist polymer and the exploitation of proper gases for enhanced milling) would permit to further decrease the exposure time of an order of magnitude or more (exposure rate $\geq 10^5$ structures/h for the considered nanotubes). However, some limitations could occur for very densely packed nanostructures. As for the minimum channel size, also the minimum pitch depends on the nanostructure shape, layout, and size. For instance, nanotubes of 1 μm in height and 150 nm in diameter can be exposed with a pitch of 300 nm. For lower pitch, the flare increases and the nanotube base tends to be stuck.

After the template fabrication, the process can continue in different ways depending on the application, as further described in Supporting Information section 1. When plasmonic nanostructures are desired, a thin layer of noble metal can be deposited on the template. In such a case, the metallic film can partially plug the channel end, resulting in a sharp bottleneck that we called waist. The waist geometry can be tuned by varying the metal deposition conditions. In addition, we notice that the metallic film covers the substrate surface as well; thus, it electrically connects one another the nanostructures and to the electrical contacts, if any, present on the chip. Furthermore, when necessary, such a metallic film can be selectively removed without damaging the structures by means of reactive ion etching, or it can be further patterned to define electrical connections.

The approach is extremely versatile and, in principle, whatever material can be deposited. By adopting a sequential deposition strategy, even multilayered coaxial structures made of different materials can be achieved (e.g., nanotube of metal/dielectric/metal; see also Supporting Information section 1).

It is important to remark that the inner hole produced by the ion milling passes through the whole nanostructure from the backside of the supporting membrane up to the tip, thus forming a nanochannel that crosses the membrane. In Figure 2, SEM pictures of a silver nanotube intentionally broken are reported to better show the inner nanochannel. Some other examples are reported in Figure 3 to show the variety of the feasible structures. Being the approach based on a top-down method (FIB), the 3D nanostructures may be fabricated in whatever 2D layout. The cross section can be circular but also squared, ellipsoidal, asymmetric, or other, and also conical or pyramidal geometries are achievable. The structures can be fabricated in the same run vertical or tilted with different angle and heights, and by crossing nanotubes arrays even nanogrids can be achieved. The nanostructures height can be increased up to few tens of micrometers, while keeping high aspect ratio between height and radius ($H/R > 70:1$, see Supporting Information section 1), hence interesting for photonic/

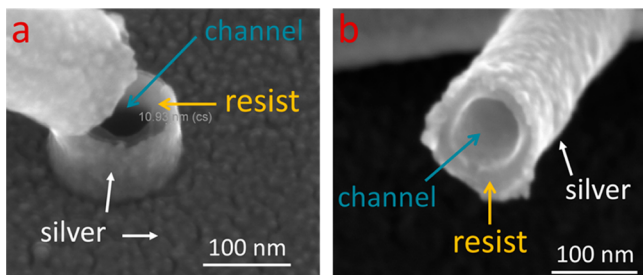


Figure 2. Plasmonic hollow nanostructures; the inner nanochannel. (a, b) SEM pictures showing a broken silver nanotube fabricated on silicon nitride membrane. The inner nanochannel crosses the whole device from the backside of the membrane, along the nanotube, up to the other side of the nanostructure. In this case, silver sidewall thickness is roughly 10 nm.

plasmonic applications from the visible up to the far-infrared and the terahertz regime.

The present method enables the fabrication of hollow nanostructures whose shape is fundamentally different from those currently achievable with conventional methods. To further analyze their distinctive features with respect to conventional planar nanostructures, we carried out a preliminary investigation of their optical properties together with numerical computations to support our analysis. We show that in addition to conventional properties of dipolar antennas (such as near field resonances and the associated electric field hot spots) their distinctive geometry enables (i) efficient excitation of high order modes that results in an effective broadband absorption, (ii) the capability of concentrating the electric field in 3D hollow nanocavities, and (iii) the capability

of connecting the plasmonic antennas to a metallic film (i.e., an electrode) without preventing their plasmonic functioning.

Among the large variety of feasible structures, we investigated the optical properties of arrays of vertical silver nanotubes fabricated on silicon nitride membrane (Figure 3, left-top panel). We considered an array of $120 \times 120 \mu\text{m}^2$ of vertical nanotubes made of silver (pitch 750 nm, height 1.1 μm , external diameter 168 nm, silver thickness on nanotube wall 18 nm, silver thickness on the substrate of 32 nm, waist 60 nm, inner core of resist with $n = 1.65$; see also Supporting Information section 3). SEM inspections reveal fabrication accuracy of ± 20 nm on nanotube height ($\pm 1.8\%$) and ± 6 nm on external radius ($\pm 5\%$). The flare at the base (increasing of nanotube radius) is less than 7% of the diameter, and by FDTD simulations we found that it does not affect significantly the optical properties. The optical transmittance at normal incidence in the ranges 360–1160 and 2100–2500 nm was measured, and the results are reported in Figure 4 (normalized with respect to the source power), together with FDTD (finite difference time domain) simulations. For a more detailed description of FDTD simulations, see Supporting Information section 4.

The nanotube array shows a finely structured transmittance profile that cannot be explained by the current theoretical approaches developed for nanocylinder, nanorods, or planar antennas.^{33,34} We anticipate that a deeper theoretical investigation is necessary to fully understand the photonic/plasmonic modal structures of the proposed architectures. However, such a study is far from the scope of this paper; therefore, here we limit to analyze the general behavior by means of FDTD computations and to outline the most

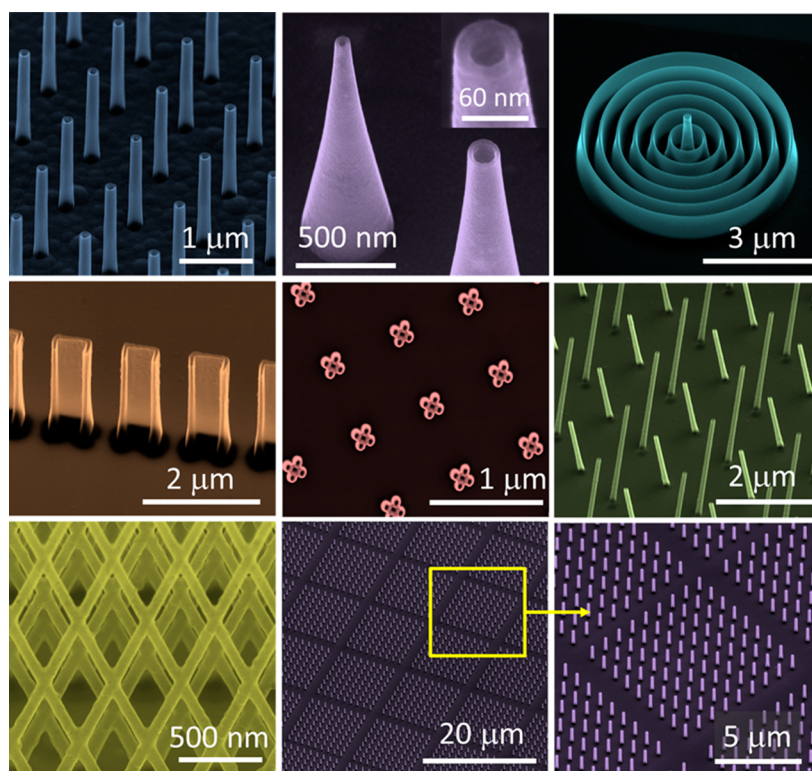


Figure 3. Fabricated hollow architectures. SEM images showing the variety of the feasible geometries. From the top left to the bottom right: vertical nanotubes and nanoneedles, 3D circular grating with a demonstrative nanoneedle in the middle, vertical structures with cross sections, tilted nanotubes with different heights and tilts, 3D nanogrid (see Figure S7 in Supporting Information for larger picture), large area nanotube arrays.

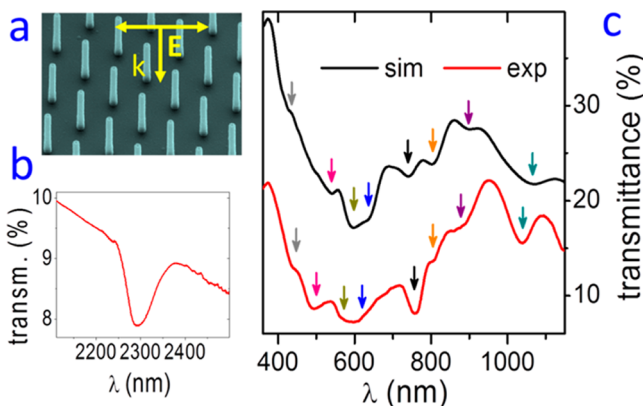


Figure 4. Transmittance of nanotube array at normal incidence. (a) SEM image of plasmonic array on silicon nitride membrane with a thin layer of silver (32 nm): height 1.1 μm , pitch 750 nm (see text and Supporting Information for a full description). (b) Nanotube array transmittance showing first-order mode at around 2290 nm. (c) Nanotube array transmittance showing higher order modes in the visible range and FDTD simulations (vertically shifted of +15% for clarity). The colored arrows indicate the main experimental peaks and the corresponding simulated peaks.

interesting novelties related to the 3D hollow shape of these nanostructures. As it can be seen in Figure 4, the transmittance profile is composed of many narrow peaks close to each other. The FDTD analysis is in good agreement with the experimental results, and it suggests that the transmittance profile is due to the overlapping of many resonant modes which can be divided into three main classes: (1) low order modes lying on the external metal surfaces; (2) high order modes resonating inside the hollow nanocavity and at the waist; (3) mixed modes as due to a combination of the previous two, thus lying on both inner and outer cylinder surfaces.

To better explain these findings, we reported in Figure 5 the electric field distribution on the nanotube for three different wavelengths (490, 590, and 890 nm) chosen as representatives of the three kinds of modes. At $\lambda = 890$ nm, the nanotube exhibits a third-order mode where the electric field resonates on the outer nanotube surface: it well represents the case of an

ideal 1D cavity usually observed in planar antennas or nanorods. The same is valid for the experimental peaks (i.e., minima of the transmittance profile) at 2290 and 1040 nm that are a first-order and second-order mode, respectively. On the contrary, at shorter wavelengths (high-order resonances), the situation is completely different. In fact, in the visible range the electromagnetic radiation penetrates inside the nanochannel (see for instance $\lambda = 490$ nm in Figure 5, fifth order). At intermediate wavelengths ($\lambda = 590$ nm in Figure 5) the electric field resonates on both inner and outer surface. Interestingly, these high-order modes are strongly confined inside the nanochannel far below the Abbe diffraction limit, thus producing a 3D plasmonic nanocavity, whose electric distribution is completely different from the one usually observed in planar antenna or nanorods.^{33,34} As it is shown in Figure 5, the electric field intensity is pretty constant in the entire volume that defines the 3D hollow nanocavity. This property is quite unusual in plasmonic antennas since they work in the near-field regime; i.e., the electric field decays rapidly in the volume far from the metal surface. As a consequence, conventional plasmonic antennas do not efficiently work in liquid or gas environment because only few molecules, those which face the metal interface, experience the near-field action. In other words, conventional plasmonic sensors are diffusion limited.³ On the contrary, in the proposed 3D hollow nanocavity, the electric field entirely fills the nanochannel; hence when gases or liquids are flowed through, they must experience the electric field action.

Another distinctive feature of the present architecture is represented by the fact that the optical excitation of the high order modes is very effective (much more than those observed in planar antennas³³). Since they are numerous and very close in wavelength, they produce a continuous extinction profile where individual resonances are no longer resolved (as it is clear in Figure 4). In general, broad band resonances allow easy excitation and absorption over a wide spectrum but poor electric field enhancement due to the limited plasmon lifetime ($\Delta\omega \approx \tau^{-1}$, where $\Delta\omega$ is the resonance width and τ the plasmon lifetime). In other words, as a rule of thumb, the narrower the resonances, the higher electric field accumulation.³⁹ Here, the continuous absorption profile is achieved by overlapping many narrower resonances whose average width $\Delta\omega$ is less than 50 nm. Therefore, the nanotubes arrays provide broad band absorption without compromising resonance quality, thus still producing good electric field enhancement over a wide spectrum. By exploiting the FDTD calculation used to reproduce the transmittance profile of Figure 4, we estimated the optical absorption of the nanotube array. Although for the considered array the geometrical cross section at normal incidence is only 3.7% of the surface area, the array absorbs 55% of the incident power in the visible spectrum with a maximum value of 83% at $\lambda = 590$ nm (Supporting Information section 4). Further optimizations are still possible, and by tuning the antennas height, radius, and arrangement, the broad band absorption can be extended up to the near/medium infrared region, improving performances of perfect infrared absorber,⁴⁰ graphene plasmonics,⁴¹ color routing, and Yagi–Uda antennas.⁴²

An additional important aspect, enabled by 3D fabrication, is the fact that the antennas come out from the substrate plane with a quasi-right angle edge at the antenna base. This is responsible for the reflection of the longitudinal standing waves, and without this edge nanocavity functioning would not be

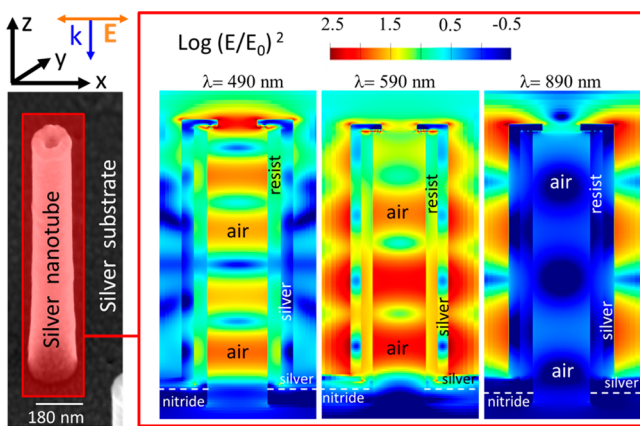


Figure 5. Theoretical analysis of nanocavity resonant modes by means of FDTD simulation. Electric field intensities along the silver nanotube cross section for three different wavelengths are shown. Inner ($\lambda = 490$ nm), outer ($\lambda = 890$ nm), and mixed mode ($\lambda = 590$ nm) are visible. Nanotube geometry is the same of the array whose transmittance is reported in Figure 4 (height 1.1 μm , radius 84 nm).

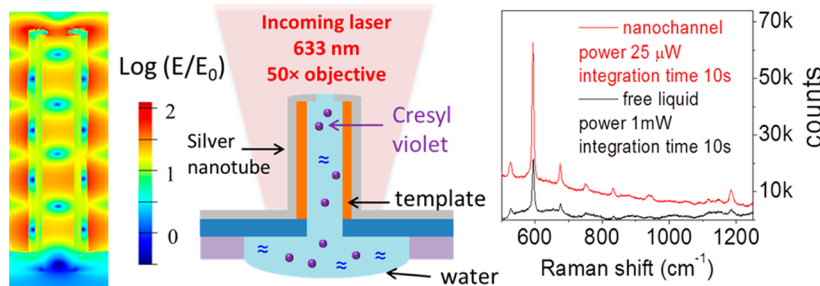


Figure 6. Raman analysis on a single nanotube (1.4 μm height, 160 nm width, 90 nm channel). Left: FDTD analysis of the electric field distribution along the nanoantennas. The cross section shows an enhancement of field amplitude of about 18 inside the nanochannel. A surface roughness on the exterior side-walls of 4 nm is taken in account. Center: sketch describing experimental setup. Right: Raman measurements performed on single nanochannel filled with a water solution of cresyl violet (1 mM). Reference spectrum is acquired on free volume of cresyl violet (1 mM). In both cases antenna excitation and signal acquisition is carried out through a 50 \times objective at normal incidence in reflection configuration ($\lambda = 633 \text{ nm}$).

possible. In fact, this *out-of-plane* architecture allows the antennas to behave as isolated nanocavities even if they are shorted by a continuous metallic layer. On the other hand, it represents a trick that makes the plasmonic nanostructures connectable to electronic circuits without cross-talk. This feature, when further developed, can be appealing in many fields that span from electrical excitation of surface plasmons⁴³ to applications in cell biology and neuroscience. In principle, such conductive hollow devices could be successfully exploited as nanoneedles for cell membrane electroporation, intracellular recording, and intracellular delivery,⁴⁴ DNA nanopore sequencing,⁴⁵ or other applications in the fields of nanomedicine and neuroscience such as multielectrode array technologies.⁴⁶

By using FDTD simulations, we further optimized the electric field enhancement for $\lambda = 633 \text{ nm}$ of both outer and inner modes on single nanotube. We found two maximum enhancement values of about 82 (nanotube waist, external surface) and 18 times (inner nanochannel) when the height is 1.4 μm and the radius is 80 nm. After that optimization, to make the simulations closer to the real devices we included a surface roughness of 4 nm on exterior side wall. The electric field inside the nanochannel and the optical transmittance seem to be not seriously affected by the introduction of surface roughness. On the contrary, the electric field enhancement at the waist shows a maximum value of about 200 times the incoming field amplitude at $\lambda = 633 \text{ nm}$ (see Figure 6). This value is far above that usually observed in planar nanostructures where nanometric gaps are necessary to provide high field enhancement. However, we consider the field confinement inside the nanochannel more novel and interesting.

Therefore, as final test to prove that the proposed hollow devices are able to work as 3D optical nanocavities, we performed Raman scattering experiments in liquid environment mimicking a microfluidic device. A water solution of cresyl violet (1 mM) was dropped on the membrane backside (see sketch in Figure 6). By recalling that the inner face of the hollow nanotubes is made of resist and that the oxygen RIE process makes the resist surface strongly hydrophilic, water solution enters and fills the nanochannel up to the waist due to capillary effect. Interestingly, this configuration helps to prevent misleading interpretation about the origin of Raman signal. In fact, there is no direct contact between the liquid solution and the metal surface except a very small region at the channel waist. Therefore, we can assume that the Raman signal is coming from the molecules dissolved in the liquid instead from molecules adsorbed into the metal surface as in ordinary SERS effect. The Raman spectrum is acquired through a 50 \times

objective on a single nanoantenna in reflection configuration ($\lambda = 633 \text{ nm}$, integration time: 10 s, laser power: 25 μW) and then compared to the signal from a free solution ($\lambda = 633 \text{ nm}$, integration time: 10 s, laser power: 1 mW). The results are reported in Figure 6. If we normalize the signal intensities with respect of scattering volume (laser focus volume and channel volume), laser power, and integration time, the signal we obtained by using the nanocavity channel is 10^4 times higher than that obtained in the free liquid under the same conditions. It means an amplification of the electric field amplitude inside the nanochannel of about 10 times the incoming electric field that is in good agreement with our simulation (as reported above, a value of 18 is estimated). This value is remarkably high if we consider that the nanocavity works in deep subdiffraction regime (radius 45 nm). It could open interesting developments in nanofluidics or in any application where high field intensity is needed in a free volume (air or liquid) of subdiffraction size. In conclusion, we presented a 3D manufacturing process based on an innovative secondary electron lithography induced by ion beam milling. The process is robust, and it is capable of defining three-dimensional hollow nanostructures with a wide variety of unconventional shapes and precise spatial arrangements. Several kinds of devices, exploitable in many different fields of basic science and technology, can be designed and fabricated. Among them, we focused our attention on arrays of vertical silver nanotubes which, thanks to their 3D shape, show different distinctive properties. In fact, being hollow, the nanochannel can work as an optical 3D nanocavity that generates inner resonant modes with a very good electric field confinement far below the Abbe diffraction limit. In particular, the overlapping of high-order modes induces efficient broad band absorption whose spectral width and position can be tuned by changing nanotube geometry. Finally, we showed that the plasmonic nanocavities are shorted by an uninterrupted metallic layer that does not prevent their plasmonic functioning, and then it paves the way to many optoelectronic applications and plasmoelectronic devices. Further theoretical and experimental studies are in progress to fully understand and to exploit both fabrication methods and device performances. However, we consider the presented results of great appealing for a wide community in different fields of science and technology.

ASSOCIATED CONTENT

Supporting Information

Sections: 1) Fabrication process; 2) Secondary electron generation by ion milling; 3) Nanotubes array details; 4)

FDTD simulation details and absorption estimation; 5) Gallium contamination evaluation. Figures S1–S12. This material is available free of charge via the Internet at <http://pubs.acs.org>.

AUTHOR INFORMATION

Corresponding Author

*E-mail: francesco.deangelis@iit.it.

Notes

The authors declare no competing financial interest.

REFERENCES

- (1) Le, F.; et al. Metallic Nanoparticle Arrays: A Common Substrate for Both Surface-Enhanced Raman Scattering and Surface-Enhanced Infrared Absorption. *ACS Nano* **2008**, *2*, 707–718.
- (2) Das, G.; et al. Nano-patterned SERS Substrate: Application for Protein Analysis vs Temperature. *Biosens. Bioelectron.* **2009**, *24*, 1693–1699.
- (3) De Angelis, F.; et al. Breaking the Diffusion Limit with Superhydrophobic Delivery of Molecules to Plasmonic Nanofocusing SERS Structures. *Nat. Photonics* **2011**, *5*, 682–687.
- (4) Stockman, M. I. Nanoplasmonics: Past, Present, and Glimpse into the Future. *Opt. Express* **2011**, *19*, 22029–22048.
- (5) Tabakman, S. M.; et al. Plasmonic Substrates for Multiplexed Protein Microarrays with Femtomolar Sensitivity and Broad Dynamic Range. *Nat. Commun.* **2011**, *2*, 466.
- (6) Wiener, A.; Fernández-Domínguez, A. I.; Horsfield, A. P.; Pendry, J. B.; Maier, S. A. Nonlocal Effects in the Nanofocusing Performance of Plasmonic Tips. *Nano Lett.* **2012**, *12*, 3308–3314.
- (7) Frontiera, R. R.; Henry, A. I.; Gruenke, N. L.; Van Duyne, R. P. Surface-Enhanced Femtosecond Stimulated Raman Spectroscopy. *J. Phys. Chem. Lett.* **2011**, *2*, 1199–1203.
- (8) Berweger, S.; Atkin, J. M.; Xu, X. G.; Olmon, R. L.; Raschke, M. B. Femtosecond Nanofocusing with Full Optical Waveform Control. *Nano Lett.* **2011**, *11*, 4309–4313.
- (9) Nikolaenko, A. E.; et al. Nonlinear Graphene Metamaterial. *Appl. Phys. Lett.* **2012**, *100*, 181109–181109-3.
- (10) Adamo, G.; et al. Electron-Beam-Driven Collective-Mode Metamaterial Light Source. *Phys. Rev. Lett.* **2012**, *109*, 217401.
- (11) Soukoulis, C. M.; Wegener, M. Past Achievements and Future Challenges in the Development of Three-Dimensional Photonic Metamaterials. *Nat. Photonics* **2011**, *5*, 523–530.
- (12) Sonnenaud, Y.; et al. Experimental Realization of Subradiant, Superradiant, and Fano Resonances in Ring/Disk Plasmonic Nanocavities. *ACS Nano* **2010**, *4*, 1664–1670.
- (13) Lassiter, J. B.; et al. Fano Resonances in Plasmonic Nanoclusters: Geometrical and Chemical Tunability. *Nano Lett.* **2010**, *10*, 3184–3189.
- (14) Thomann, I.; et al. Plasmon Enhanced Solar-to-Fuel Energy Conversion. *Nano Lett.* **2011**, *11*, 3440–3446.
- (15) Hung, W. H.; Aykol, M.; Valley, D.; Hou, W.; Cronin, S. B. Plasmon Resonant Enhancement of Carbon Monoxide Catalysis. *Nano Lett.* **2010**, *10*, 1314–1318.
- (16) Neumann, O.; Urban, A. S.; Day, J.; Surbhi, L.; Nordlander, P.; Halas, N. Solar Vapor Generation Enabled by Nanoparticles. *ACS Nano* **2013**, *7*, 42–49.
- (17) Liu, Z.; Hou, W.; Pavaskar, P.; Aykol, M.; Cronin, S. B. Plasmon Resonant Enhancement of Photocatalytic Water Splitting Under Visible Illumination. *Nano Lett.* **2011**, *11*, 1111–1116.
- (18) Atwater, H. A.; Polman, A. Plasmonics for Improved Photovoltaic Devices. *Nat. Mat.* **2010**, *9*, 205–213.
- (19) Khajavikhan, M.; et al. Thresholdless Nanoscale Coaxial Lasers. *Nature* **2012**, *482*, 204–207.
- (20) Stockman, M. I. Spaser Action, Loss Compensation, and Stability in Plasmonic Systems with Gain. *Phys. Rev. Lett.* **2011**, *106*, 156802.
- (21) Baffou, G.; Quidant, R.; Garcìa de Abajo, F. J. Nanoscale Control of Optical Heating in Complex Plasmonic Systems. *ACS Nano* **2010**, *4*, 709–716.
- (22) Novotny, L.; et al. Theory of Nanometric Optical Tweezers. *Phys. Rev. Lett.* **1997**, *79*, 645.
- (23) Juan, M. L.; Righini, M.; Quidant, R. Plasmon Nano-optical Tweezers. *Nat. Photonics* **2011**, *5*, 349–356.
- (24) De Angelis, F.; et al. Nanoscale Chemical Mapping Using Three-Dimensional Adiabatic Compression of Surface Plasmon Polaritons. *Nat. Nanotechnol.* **2010**, *5*, 67–72.
- (25) Fleischer, M.; et al. Gold Nanocone Near-Field Scanning Optical Microscopy Probes. *ACS Nano* **2011**, *5*, 2570–2579.
- (26) Wei, Bao; et al. Mapping Local Charge Recombination Heterogeneity by Multidimensional Nanospectroscopic Imaging. *Science* **2013**, *338*, 1317–1321.
- (27) De Angelis, F.; Proietti, R. Z.; Di Fabrizio, E. Mapping the Local Dielectric Response by Means of Plasmonic Force Spectroscopy. *Opt. Express* **2012**, *20*, 29626–29633.
- (28) Fan, X.; White, I. M. Optofluidic Microsystems for Chemical and Biological Analysis. *Nat. Phot.* **2011**, *5*, 591–597.
- (29) Erickson, D.; Sinton, D.; Psaltis, D. Optofluidics for Energy Applications. *Nat. Photonics* **2011**, *5*, 583–590.
- (30) Fang, Z.; Liu, Z.; Wang, Y.; Ajayan, P. M.; Nordlander, P.; Halas, N. J. Graphene-Antenna Sandwich Photodetector. *Nano Lett.* **2012**, *12*, 3808–3813.
- (31) Cai, W.; Vasudev, A. P.; Brongersma, M. L. Electrically Controlled Nonlinear Generation of Light with Plasmonics. *Science* **2011**, *333*, 1720–1723.
- (32) Esteban, R.; Borisov, A. G.; Nordlander, P.; Aizpurua, J. Bridging Quantum and Classical Plasmonics with a Quantum-Corrected Model. *Nat. Commun.* **2012**, *3*, 825.
- (33) Dorfmüller, J.; et al. Plasmonic Nanowire Antennas Experiment, Simulation, and Theory. *Nano Lett.* **2010**, *10*, 3596–3603.
- (34) Novotny, L.; Hafner, C. Light Propagation in a Cylindrical Waveguide with a Complex Metallic Dielectric Function. *Phys. Rev. E* **1997**, *56*, 4094–4108.
- (35) McPhillips, J.; et al. High-Performance Biosensing Using Arrays of Plasmonic Nanotubes. *ACS Nano* **2010**, *4*, 2210–2216.
- (36) Li, J.; Stein, D.; McMullan, C.; Branton, D.; Aziz, M. J.; Golovchenko, J. A. Ion-Beam Sculpting at Nanometer Length Scales. *Nature* **2001**, *412*, 166–169.
- (37) Brian Leen, J.; Hansen, P.; Cheng, Y.-T.; Hesselink, L. Improved Focused Ion Beam Fabrication of near-Field Apertures Using a Silicon Nitride Membrane. *Opt. Lett.* **2008**, *33*, 2827–2829.
- (38) Patterson, N.; Adams, D. P.; Hodges, V. C.; Vasile, M. J.; Michael, J. R.; Kotula, P. G. Controlled Fabrication of Nanopores Using a Direct Focused Ion Beam Approach with Back Face Particle Detection. *Nanotechnology* **2008**, *19*, 235304.
- (39) Garcia de Abajo, F. J. Light Scattering by Particle and Hole Arrays. *Rev. Mod. Phys.* **2007**, *79*, 1267–1290.
- (40) Liu, N.; Mesch, M.; Weiss, T.; Hentschel, M.; Giessen, H. Infrared Perfect Absorber and Its Application as Plasmonic Sensor. *Nano Lett.* **2010**, *10*, 2342–2348.
- (41) Fang, Z.; et al. Gated Tunability and Hybridization of Localized Plasmons in Nanostructured Graphene. *ACS Nano* **2013**, *7*, 2388–2395.
- (42) Kosako, T.; Kadoya, Y.; Hofmann, H. F. Directional Control of Light by a Nano-optical Yagi–Uda Antenna. *Nat. Photonics* **2010**, *4*, 312–315.
- (43) Bharadwaj, P.; Bouhelier, A.; Novotny, L. Electrical Excitation of Surface Plasmons. *Phys. Rev. Lett.* **2012**, *106*, 226802.
- (44) Shalek, A. K.; et al. Vertical Silicon Nanowires as a Universal Platform for Delivering Biomolecules into Living Cells. *Proc. Natl. Acad. Sci. U. S. A.* **2010**, *107*, 1870–1875.
- (45) Venkatesan, B. M.; Bashir, R. Nanopore Sensors for Nucleic Acid Analysis. *Nat. Nanotechnol.* **2011**, *6*, 615–624.
- (46) Spira, M. E.; Hai, A. Multi-electrode Array Technologies for Neurosciences and Cardiology. *Nat. Nanotechnol.* **2012**, *8*, 83–94.